



EFFECT OF FRICTION STIR PROCESSING ON THE MICROSTRUCTURE AND MECHANICAL PROPERTIES OF IRON-BEARING A356 CAST ALUMINUM ALLOY

Behzad Asharsheikh and Mohammad H. Daneshifar 10

Department of Materials Engineering, Hakim Sabzevari University, Sabzevar 9617976487, Iran

Mohammad A. Jabbareh

Department of Materials Engineering, Hakim Sabzevari University, Sabzevar 9617976487, Iran
Department of Materials Science and Engineering, Engineering Faculty, Ferdowsi University of Mashhad, Azadi Square,
Mashhad, Iran

Copyright © 2025 American Foundry Society https://doi.org/10.1007/s40962-025-01557-z

Abstract

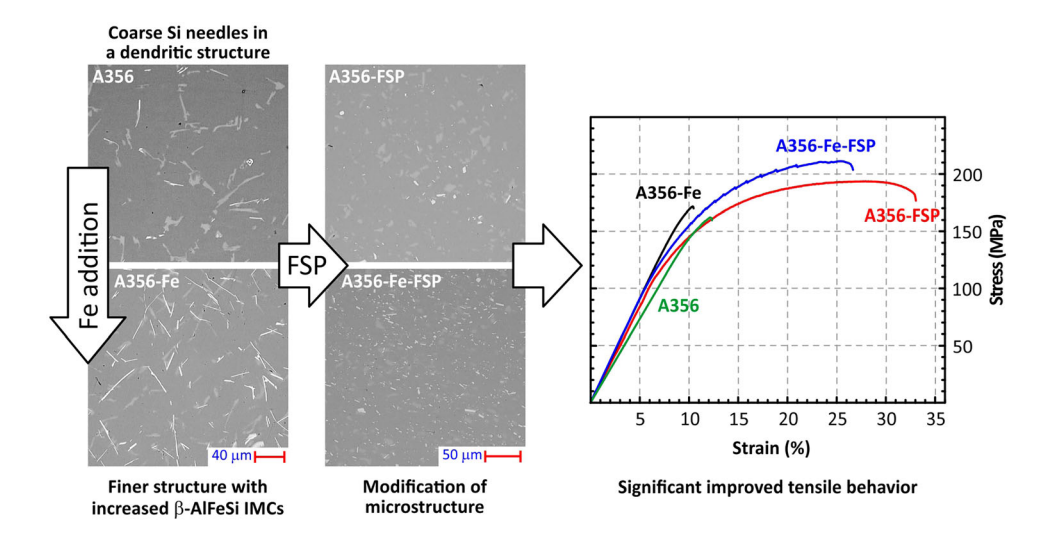
In the recycled aluminum alloys, iron is the most common impurity, usually deleterious to their mechanical properties, especially the ductility of the alloys. In this study, effect of friction stir processing (FSP) was studied on the microstructure and mechanical properties of standard and Fe-bearing A356 cast Al alloys. For this purpose, A356 and A356–1.2 wt.% Fe base metals were prepared in the form of plates by gravity casting in a steel mold and FSPed with parameters 1000 rpm rotational speed, 50 mm/s traverse speed, 2° tool tilting angle, and 0.2 mm plunging depth. The microstructure and mechanical properties of FSPed samples were studied and compared to those of the as-cast base metals. The results revealed that addition of

Fe to A356 refined microstructure and increased fraction of acicular β-AlFeSi intermetallic compounds (Fe-IMCs) which in turn increased strength (6%) but reduced ductility (15%) of A356-Fe base metal compared to the standard A356. FSP fragmented both acicular Si and Fe-IMCs and redistributed them uniformly in the structure. The FSPed sample containing 1.2 wt.% Fe shows tensile strength as high as 211 MPa and at the same time elongation of 25% which are 23% and 147% higher than those of the cast base metal. The present results prove the beneficial effects of FSP on the problems associated with Fe residue in the recycled Al alloys.

Received: 02 September 2024 / Accepted: 15 January 2025

Published online: 28 February 2025

Graphical Abstract



Keywords: cast Al-Si alloy, iron-bearing intermetallics, friction stir processing, microstructure, hardness, tensile properties

Introduction

Mechanical and tribological properties of cast aluminum alloys strongly depend on their microstructure. Amongst cast Al alloys, Al-Si alloys find extensive applications because of low cost, good castability, high specific properties, and excellent tribological behavior. Mechanical properties of these alloys are mainly determined by fraction, distribution, and morphology of silicon particles in α –Al matrix. It was shown that good mechanical and tribological properties can be achieved by fine, rounded, and homogeneously distributed Si particles. However, their cast structure usually contains coarse needles of Si which strongly reduce the ductility of the alloy.

Recycling is a very important aspect of Al industries in recent years because of the limited resources and need for sustainable materials management. In the recycled Al alloys, iron is considered as the main impurity element.³ Iron can form several types of intermetallics (Fe-IMCs) in cast alloys such as α-Al₈Fe₂Si script-like phase, β-Al₅FeSi platelet, and π-Al₈FeMg₃Si₆ phase among other less important phases.⁴ It has been reported that, similar to Si needles, these intermetallic phases, especially β platelets, have strong effect on the properties of Al castings.^{5–7} Hence, the control of morphology and modification of Si and Fe containing intermetallic compounds are essential. To this end, different techniques were developed including heat treatment, 2,8 chemical method, 9,10 and dynamic methods. 11-13 Among these methods, the chemical method is the most commonly method, in which, different alloying elements added to the Al alloys melt. For instance, strontium commonly used to modify the morphology of Si needles, 14 while Mn is known as strong modifier for Fe-IMCs. 7 Khan and his colleagues 15 studied the effects of addition of 0.5% Mn on the Fe-IMCs in 6082-1% Fe and

Table 1. Chemical Composition of the Cast Alloys

Alloy	Concentration (wt.%)								
	Si	Mg	Fe	Cu	Mn	Zn	Ca	Ti	Al
Standard A356	6.5–7.5	0.25-0.45	Max 0.2	Max 0.2	Max 0.1	Max 0.1	_	Max 0.2	Rem.
A356	6.591	0.384	0.171	0.002	0.010	0.016	0.004	0.008	Rem.
A356-Fe	6.682	0.146	1.220	0.264	0.031	0.169	800.0	0.012	Rem.

revealed that the addition of Mn can change morphology of β-Al₉Fe₂Si₂ platelets into α-Al₁₅(Fe, Mn)₃Si₂ Chinese script. Tzeng et al. 16 investigated the effects of Sc additions on the Fe-IMCs in Al-7Si-0.6Mg alloy. They observed that addition of Sc to the base alloy transforms β-Al₅FeSi phase into a harmless Sc-Fe nodular phase $(Al_{12}Si_6Fe_2(Mg, Sc)_5)$ which caused ~ 110% improved ductility compared to the base alloy. ¹⁶ Another strategy to modify Fe-IMCs is increasing the cooling rate during solidification. Wang et al. 17 studied the effects of Sr addition and cooling rate on the morphology of Si and Fe-IMCs in A380 alloy and observed that addition of Sr and increasing the cooling rate during solidification change the morphology of β platelets and also transfer morphology of β platelets to α script-like phase. Although chemical methods gain success in modifying the Si and Fe-IMCs, they introduce impurity to the alloy, and they may worsen other aspects of the microstructure. For example, addition of Sr can greatly modify Si morphology, 10 but it has minor effect on Fe-IMCs⁷ and can increase hydrogen adsorption to the melt. 10 Other technics also have its own limitations. For example, heat treatment can change Si needles to granular Si particles, but it needs long-time exposure of the parts at relatively high temperatures.^{2,8}

Friction stir processing (FSP) shows promising results in distribution of grain size and second phases, ^{18–21} especially the homogenization of cast structures. ²² It is quick with low energy consumption and no pollution, hence known as a green and nature friendly processing method. Numerous scientists were employed FSP to modify cast structure of aluminum alloys and matrix composite (AMCs) in solid state. ^{22–28} In general, it was observed that high temperature

and shear associated with FSP causes i) elimination of dendritic structure, ii) significant refinement and uniform distribution of Si particles, and iii) elimination of casting defects (such as holes and segregation) in the stirred zone (SZ).^{22,23} The microstructural modification by FSP results in considerable improvement of tensile properties^{24,29} and wear behavior^{25,30} of the SZ.

Based on the above literature review, although FSP showed significant improvement in structure and properties of Al-Si alloys, a systematic study on Al-Si alloy containing considerable amounts of Fe impurity is missing. Hence, the aim of the present study is to investigate the effect of FSP process on the microstructure and mechanical properties of Al-Si cast alloys with and without Fe additions. Accordingly, a very common Al-Si-Mg cast hypoeutectic alloy (A356) was selected as the base and A356 + 1.2 wt.% Fe, was prepared as Fe-bearing alloy by casting. Both A356 and A356-Fe alloys were FSPed with the same FSP parameters. To investigate the effect of Fe addition and FSP, the microstructure and mechanical properties of

Table 2. Samples Codes and the Preparation Conditions

Sample code	Alloy	Condition
A356	A356	Cast
A356-FSP	A356	FSPed
A356-Fe	A356-1.2 wt.% Fe	Cast
A356-Fe-FSP	A356-1.2 wt.% Fe	FSPed

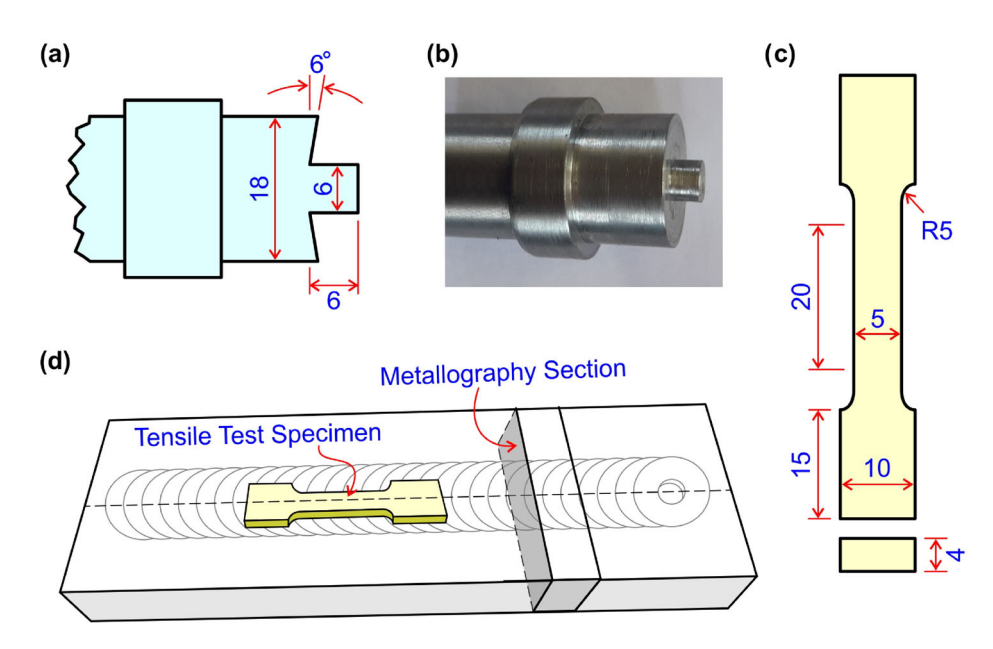


Figure 1. (a) Schematic drawing and (b) digital image showing the FSP tool geometry and dimensions, (c) geometry and dimensions of tensile test specimen, and (d) location of metallography and tensile test specimens. All dimensions are in millimeters.

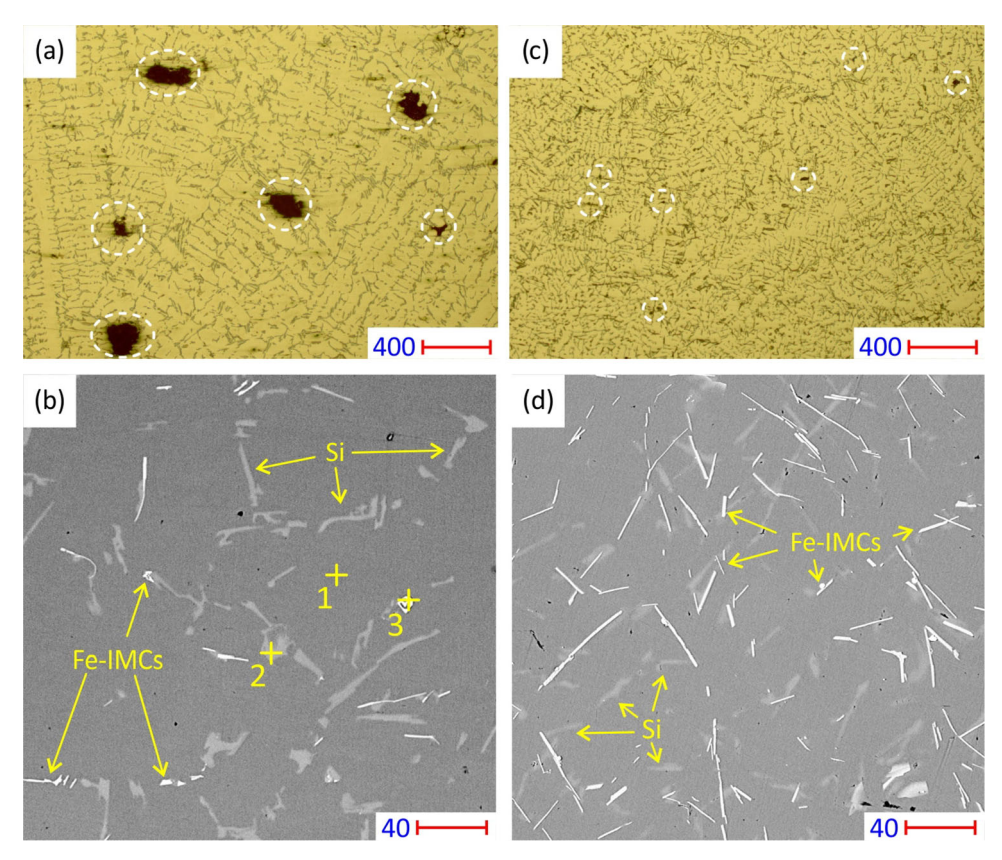


Figure 2. Optical/SEM micrographs of the as-cast microstructures of (a) and (b) A356 and (c) and (d) A356-Fe. The holes are marked by dashed circles. Scale bar values are in microns. Optical and SEM micrographs are at $50\times$ and $1000\times$, respectively.

Table 3. Results of SEM/EDS Point Analysis for the Points Indicated in Figure 2 (b)

Spectrum number	Compositions (wt.%)					
	Si	Fe	Mg	Mn	Al	
1	1.3	0.1	0.1	0.0	98.5	
2	95.3	0.1	0.5	0.1	4.0	
3	17.4	14.4	0.7	0.2	67.3	

FSPed samples were studied and compared to those of the cast base metals.

Experimental Procedure

Materials

In this research, cast and FSPed A356 Al-Si-Mg samples containing 1.2 wt.% Fe were prepared, and their mechanical behaviors were compared with cast and FSPed standard A356 samples. The addition of 1.2 wt.% Fe was selected based on the literature. A356 ingot, commercially pure Si, and Al-10 wt.% Fe master alloy were

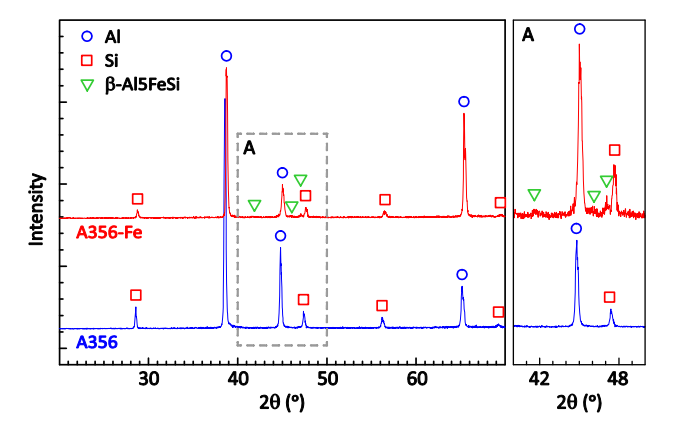


Figure 3. XRD patterns of cast A356 and A356-Fe base metals.

used as raw materials. In order to prepare 2 kg of Febearing A356 alloy, pre-weighted raw materials were melted in a silicon carbide crucible by an induction furnace. The melt was cast, at 700 °C, in a Y-block steel mold preheated to 450 °C to form a slab with dimensions (length \times width \times thickness) 250 \times 150 \times 12 mm. The cast slab was then cut into plates with dimensions of (length \times width \times thickness) 150 \times 40 \times 12 mm for FSP. Chemical

Table 4. Results of Quantitative Metallography

Sample code	Si particles		Fe-IMCs			
	Average length (μm)	Size reduction (%)	Average length (μm)	Size reduction (%)	Volume fraction (%)	
A356	13.2	_	6.2	_	0.7	
A356-FSP	3.9	70	4.1	34		
A356-Fe	12.9	_	8.1	_	6.3	
A356-Fe-FSP	3.5	73	3.6	56	_	

composition of the alloys was measured by optical emission spectroscopy (OES) and reported in Table 1. Based on the data in the table, it can be seen that, while the composition of A356 alloy lies within the standard range, A356-Fe alloys slightly deviate from the standard range. This will be discussed in the future sections.

FSP Practice

FSP was conducted using a Machine Sazi Tabriz FP4M universal milling machine. A tool with geometry and dimensions shown in Figure 1a, b made of H13 hot working tool steel was employed for FSP. FSP parameters were selected according to the literature and several trial pretests. ^{30,34} The FSP parameters were 1000 rpm rotational speed, 50 mm/min traverse speed, 2° tool tilting angles, and 0.2 mm plunging depth and kept constant for all FSP runs. Samples codes are listed in Table 2.

Characterization

Microstructures of the samples were studied on the cross sections cut from the same locations of the processed plates according to Figure 1d. Metallography samples were prepared by conventional methods include grinding by 60–1500 grit abrasive papers, polishing with 1 μm diamond paste, and for higher contrast, etched using 1% HF solution for 10–15 s. Microstructural examinations were performed by Olympus GX51 optical microscope and TESCAN Mira3 field emission scanning electron microscope (FE-SEM) equipped with EDS detector. Quantitative metallography was conducted on both optical and SEM micrographs by image analysis using MIP4 software. In order to identify the phases formed in the cast samples, XRD test were conducted on the same sections used for metallography by Philips PW1730.

Vickers hardness profiles were measured by a Qualitest QV-1000 microhardness testing machine with 100 g force and 10 s dwell time. The hardness profiles were measured on a straight path, 2 mm below the surface and 500 μ m distance between the two adjacent indentations. One profile





Figure 4. Appearance of the FSPed plates (a) A356-FSP and (b) A356-Fe-FSP.

was measured for each sample, containing at least 40 indentations.

Tensile tests were performed according to ASTM E8 by a Zwick/Roell Z250 machine. For FSPed samples, tensile test specimens were prepared from the stirred zone (Figure 1d). All tensile test specimens were cut precisely by wire-cut EDM with the geometry and dimensions presented in Figure 1c. Two tensile tests were performed for each sample. Fractured surfaces of tensile tests specimens were also studied by the FE-SEM used for metallography.

Results and Discussion

Structure of the Cast Base Metals

Microstructures of the cast base metals are presented in Figure 2. In this figure, images (a) and (c) are optical micrographs showing the general structure at very low magnification and images (b) and (d) are backscattered (BSE) SEM micrographs showing the detailed microstructure at higher magnification. It can be seen from the Figure 2a that A356 sample shows dendritic structure of α -Al phase with some α -Al + Si eutectic mixture in the

interdendritic regions. This sample also contains large voids as a result of casting solidification. Based on the Figure 2b and EDS results presented in Table 3, and XRD pattern in Figure 3, three phases can be distinguished in the microstructure including primary α –Al phase (matrix), Si needles (light gray phases), and some Fe-IMCs (white phases). The formation of Fe-IMCs is because the commercial A356 alloy employed in this research already contains ~ 0.17 wt.% Fe, (as reported earlier in Table 1). This is known as the general structure of an unmodified cast A356 Al-Si alloy. Results of quantitative metallography are reported in Table 4. According to Figure 2c, d, increasing the Fe content to the 1.22 wt.% in sample A356-

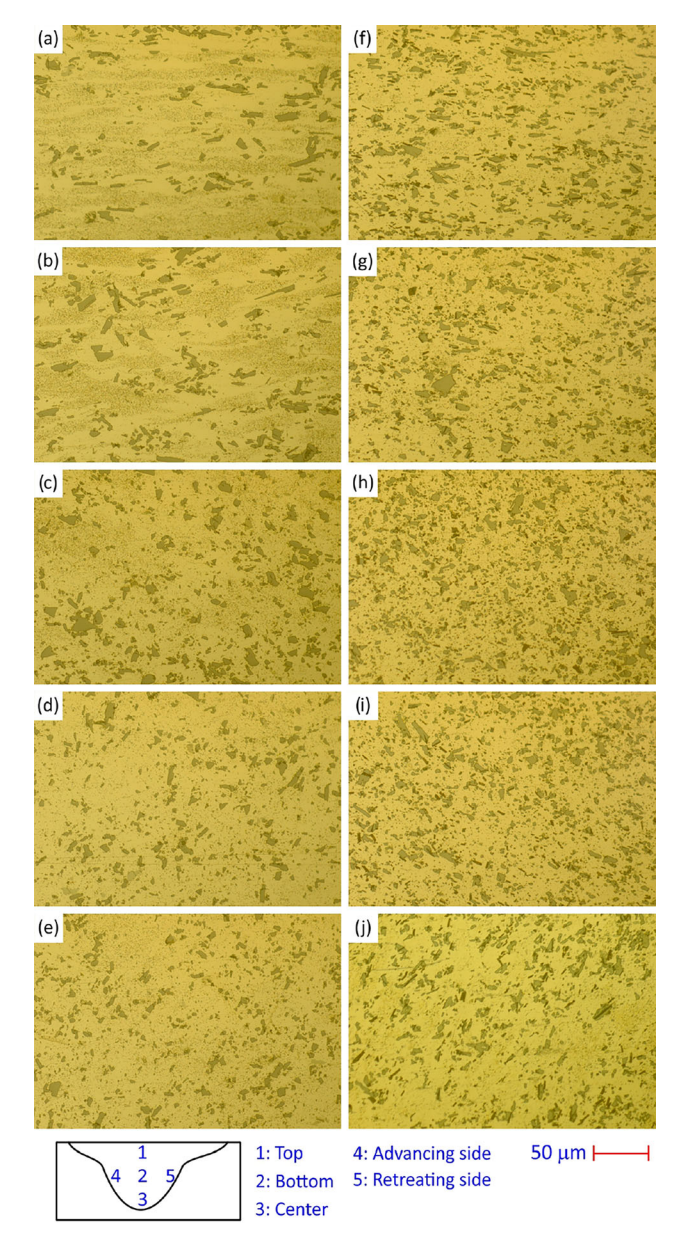


Figure 5. Optical micrographs showing the microstructure of SZ. (a)–(e) top, center, bottom, RS, and AS of the A356-FSP sample and (f)–(j) top, center, bottom, RS, and AS of the A356-Fe-FSP sample, respectively. Magnification is 500×.

Fe, causes remarkable refinement of the dendritic microstructure and considerably increases the fraction of Fe-IMCs. Based on the data in Table 4, addition of 1.2 wt.% Fe to the base metal, increased the fraction of Fe-IMCs from 0.7 to 3.1 vol.%. Average Si needle length was also reduced slightly; however, average Fe-IMCs length was considerably increased from 6.2 to 8.1 μ m (30% increase). Interestingly, it was also observed that the A356-Fe sample contains small interdendritic porosities instead of large voids in A356 sample.

The microstructure refinement of an alloy by altering its chemical composition is best explained by the growth restriction theory. It has been reported that the growth restriction factor for Fe atoms in Al is relatively high¹⁵ suggesting that, adding around 1 wt.% Fe to the base alloy, can significantly refine its microstructure. Additionally, Table 1 indicates that in the A356-Fe sample, not only Fe but also other alloying elements such as copper (Cu), zinc (Zn), calcium (Ca), and titanium (Ti) were present in higher amounts compared to the A356 sample. These elements originate from the Al-Fe master alloy and can enhance the growth restriction effect of Fe. Among these elements, Ti is particularly an effective grain refiner, although it has little impact on the morphology and size of Si and β-AlFeSi phases.³⁵ While Ca can act as eutectic modifier, it is less effective than the conventionally used Sr element. Furthermore, based on Figure 2 and Table 4, no modification effect on Si morphology was observed. So it can be concluded that the amount of Ti and Ca does not have a profound effect on the morphology and size of Si and β-AlFeSi phases.

Experimental observations on phase formation in cast base metals were confirmed by thermodynamic calculations using OpenCalphad software with COST 507 database. In A356 alloy, the phases (by weight fraction) are α -Al (92.5%), Si (6.3%), β-AlFeSi (0.6%), and Mg₂Si (0.6%). In contrast, the A356-Fe sample contains α-Al (88.8%), Si (5.9%), β-AlFeSi (4.5), Al₅Cu₂Mg₈Si₆ (0.5%), and Al₂Cu (0.3%). It can be seen that the change in chemical composition of the alloy significantly altered the fraction of β-AlFeSi which is consistent with experimental results. Additionally, minor phases in the microstructure were affected, with Mg₂Si being replaced by Al₅Cu₂Mg₈Si₆ and Al₂Cu. Based on the literature, although Al₅Cu₂Mg₈Si₆ has a weaker strengthening effect than Mg₂Si, the presence of both Al₅Cu₂Mg₈Si₆ and Al2Cu together may significantly enhance the alloy's strength due to a synergistic strengthening effect.

XRD patterns of cast base metals are presented in Figure 3. According to the XRD patterns, peaks of Al (JCPDS No. 00-004-0787) Si (JCPDS No. 01-077-2111), and β -Al₅FeSi (supported by literature³⁶), are present in the pattern. These include Al peaks at 2θ values around 38.5 (Al 111), 44.8 (Al 200), and 65.3 (Al 220), Si peaks at 2θ values about

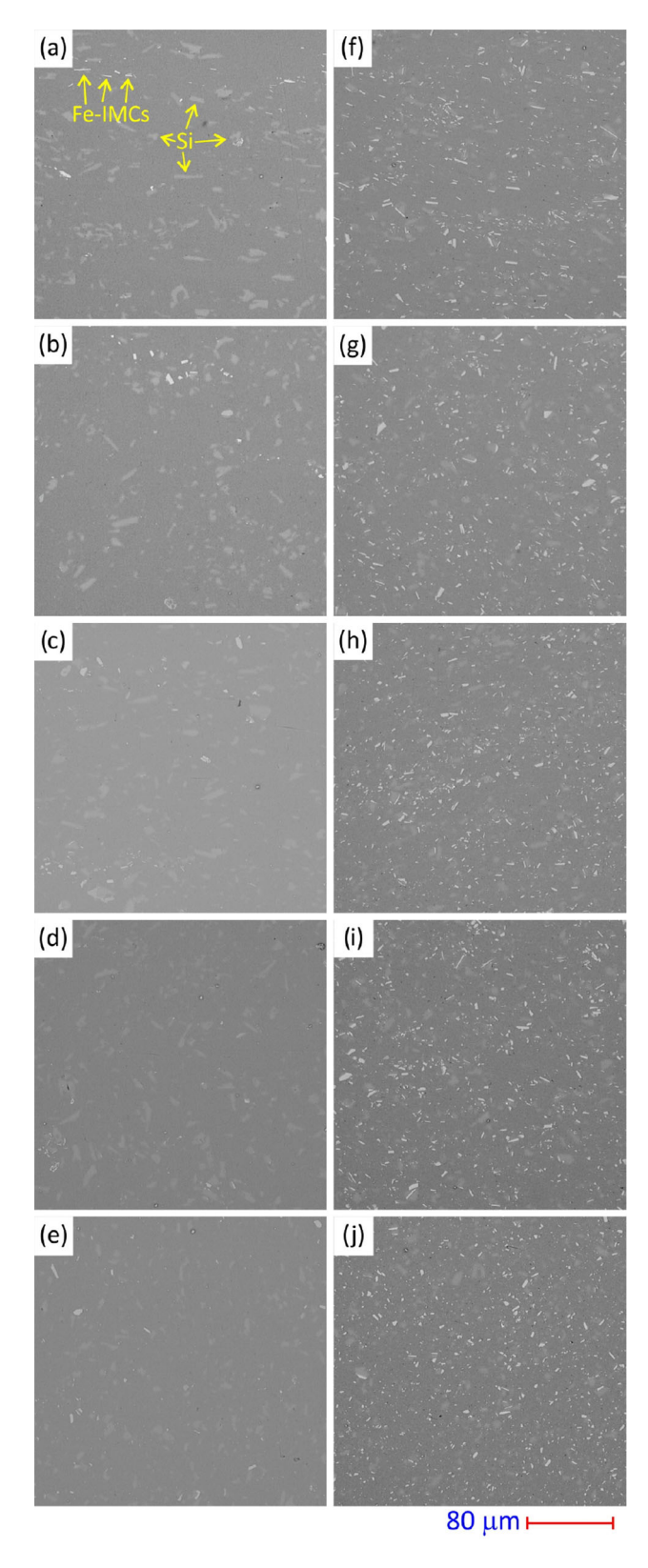


Figure 6. SEM micrographs showing the microstructure of the SZ of (a)–(e) top, center, bottom, RS, and AS of the A356-FSP sample and (f)–(j) top, center, bottom, RS, and AS of the A356-Fe-FSP sample, respectively. Magnification is 1000×.

28.5 (Si 111), 47.5 (Si 200), 56.3 (Si 311), and 69.5 (Si 400), and β -Al₅FeSi peaks at 2 θ values around 41.7, 46.0, and 47.1. A slight peak shift toward higher 2θ values was noticed in the XRD pattern of A356-Fe compared to that of A356 alloy. Such peak shifts are usually attributed to changes in the phase's chemistry. It is well-known that the dissolution of atoms with a higher atomic radius shifts peaks to lower 20 values, and vice versa. Based on the chemical composition in Table 1, it is observed that the concentrations of Mg and Zn in A356-Fe differ from those in A356 alloy. Decreasing Mg concentration and increasing Zn concentration cause the α -Al peaks to shift to higher 2θ values. According to Bragg's rule, the lattice parameter for α-Al in A356 and A356-Fe alloys are calculated to be 4.044 Å and 4.026 Å, respectively, while the lattice parameter for Si in A356 alloy is calculated to be 5.024 Å.

Structure of the FSPed Samples

Digital images of the FSPed plates are shown in Figure 4. The appearance of the FSPed surfaces is very smooth and free of any macro defects. Some flashes are formed, mainly at the retreating side of the stirred zone.

Optical micrographs showing the microstructure at different locations of the stirred zone (SZ) are presented in Figure 5. According to Figure 5a-e, it can be seen that in sample A356-FSP, the coarse Si needles are broken into small Si particles as a results of severe shear strain and high temperature accommodated with the FSP process. The α -Al dendrites are also broken and fragmented Si particles distributed more uniformly inside the α -Al matrix. It should be mentioned that although the microstructure homogeneity increases as a result of FSP, but it is apparent from the micrographs that the size distribution of Si fragmented particles are different at different locations of the SZ. It can be seen that among different locations in the SZ, center of SZ shows the coarsest structure and advancing side shows the finest structure. This gradient in the microstructure was also observed and reported by other researchers and Al-Si³⁷ and Al 7050,³⁸ and attributed to nonuniform shear strain and temperature gradients within the SZ. Shear strain is maximum close to the FSP tool surface, ³⁹ i.e., top (just below the tool shoulder) and the retreating (RS) and advancing (AS) sides. The temperature is highest at the top and the centerline of the SZ and lowest at the RS and AS of the SZ.40 Increasing the shear strain tends to refine the microstructure, whereas increasing the temperature tends to coarsen it. Therefore, the size of microstructure in different regions of the SZ will be determined by the balance between these opposing effects. In sample A356-Fe-FSP, the same trend can be seen with the difference that the structure is finer due to the cast structure was finer as it was already presented in Figure 2b. The broken Fe-IMCs are better presented in SEM micrographs shown in Figure 6. It can be seen that the same

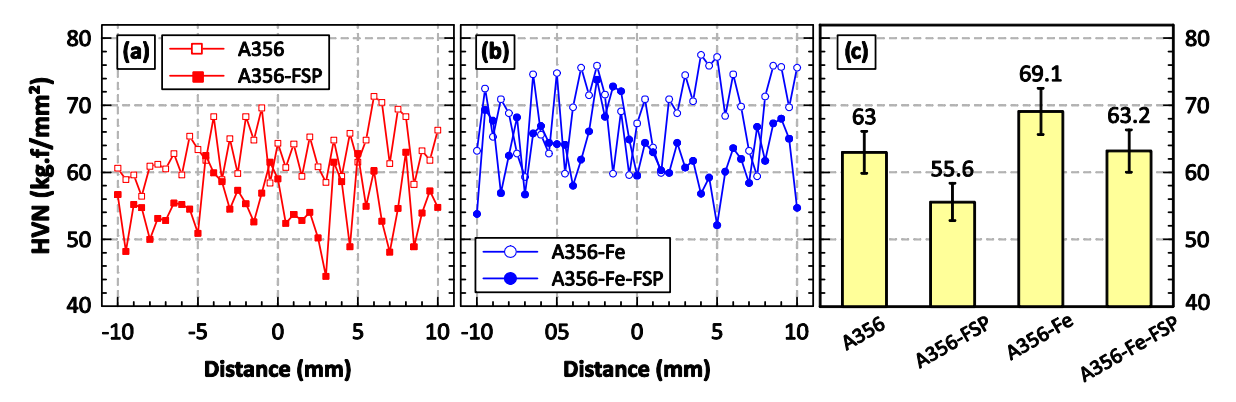


Figure 7. Hardness profiles of (a) Fe-free samples, (b) Fe-bearing samples, and (c) average hardness value (for FSPed samples average hardness of SZ).

Sample code Average hardness Tensile stress Elongation (HVN) (MPa) Uniform (%) Total (%) A356 63.0 ± 3.7 162.1 ± 18.8 12.2 ± 2.5 12.3 ± 2.5 A356-FSP 55.6 ± 4.3 193.7 ± 15.9 28.0 ± 3.7 33.0 ± 4.3 A356-Fe 69.1 ± 5.7 171.5 ± 20.8 $10.5\,\pm\,2.2$ 10.3 ± 2.2 A356-Fe-FSP 63.1 ± 5.0 211.3 ± 19.7 25.4 ± 3.8 26.7 ± 4.1

Table 5. Results of Mechanical Tests

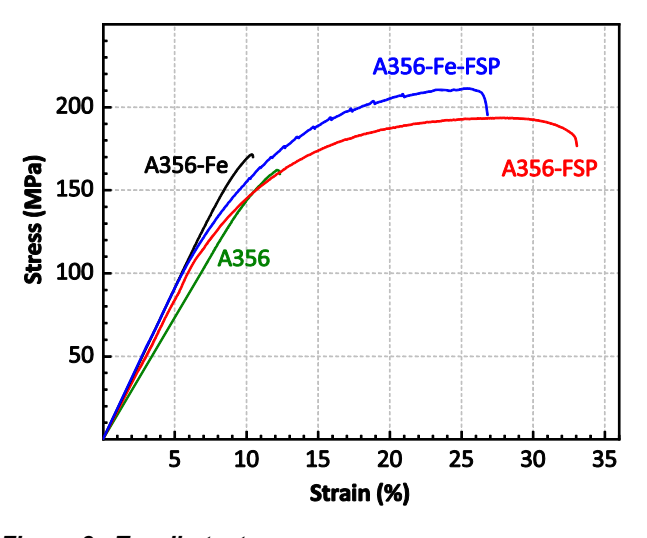


Figure 8. Tensile test curves.

phenomena occurred for the Si needles also happens to the Fe-IMCs needles. This proves the benefit of FSP method over chemical methods in which works the same for both of the needle shaped phases, i.e., Si and Fe-IMCs. Results of quantitative metallography in SZ of FSPed samples are also presented in Table 4. It can be seen that FSP considerably refines the Si and Fe-IMCs needles. Regardless of initial size of the needles, the average size of fragmented particles is at 3.5–4.2 µm range. Si needles were refined by 70% and Fe-IMCs by 34–55%. It was also observed that the degree of refinement is more pronounced in A356-Fe-

FSP compared to A356-FSP, as a result of finer initial cast structure.

Hardness

Results of hardness measurements are shown in Figure 7 and Table 5. It can be seen that Fe-bearing samples show higher hardness than that of Fe-free samples. It was also observed that FSPed samples exhibit lower hardness than that of the cast alloys. In the case of A356 sample, the average hardness is ~ 63 HVN which is reduced to 55.6 HVN in the A356-FSP sample (11.7% reduction). For A356-Fe sample, the average hardness is 69.1 HVN which reduces to 63.2 HVN in A356-Fe-FSP sample (8.5%) reduction). Addition of Fe considerably refines the structure of Fe-bearing samples, as already shown in Figs 2 and 6. Fraction of hard second phases is also higher in Febearing samples. These can be the reasons for the observed higher hardness in Fe-bearing samples. Reduction of hardness in FSPed samples compared to cast samples was also observed by other researchers and is due to dissolution of Mg₂Si precipitates.²³

Tensile Properties

Engineering stress-strain curves resulted from tensile tests are presented in Figure 8. The data extracted from the

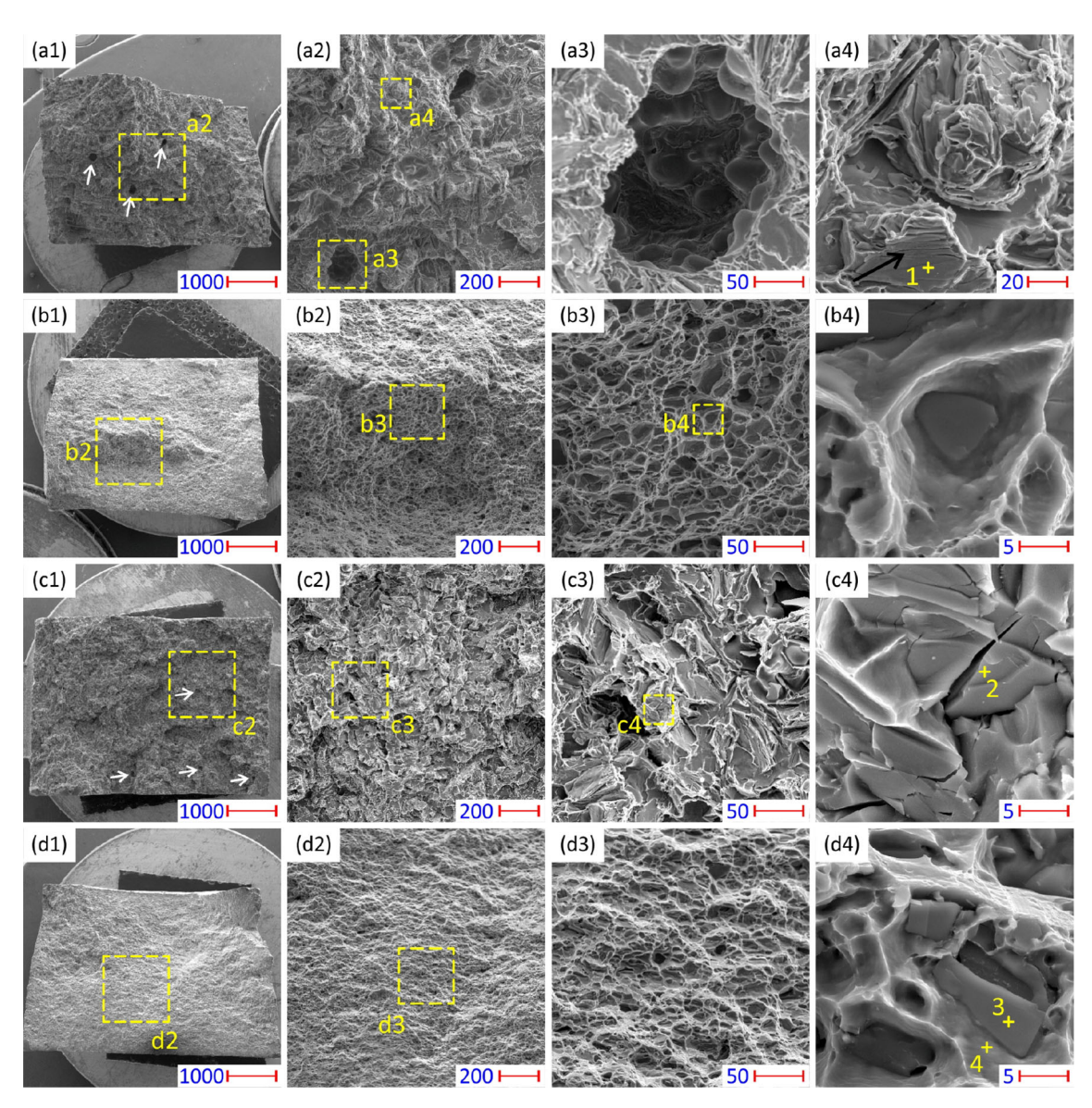


Figure 9. SEM micrographs showing the fractured surfaces of the tensile test specimens. (a1–a4) A356, (b1–b4) A356-FSP, (c1–c4) A356-Fe, and (d1–d4) A356-Fe-FSP. Scale bar values are in microns.

Table 6. Results of SEM/EDS Point Analyses for the Points Indicated in Figure 9

Spectrum number	Compositions (wt.%)				
	Si	Fe	Mg	Al	
1	95.2	0.1	0.5	4.2	
2	19.7	47.1	0.1	33.1	
3	16.8	21.7	0.4	61.1	
4	1.2	0.1	0.9	97.8	

tensile tests are reported in Table 5. It can be seen that addition of Fe to the A356 sample increased tensile strength from 162.1 MPa to 171.5 (6% increase), but

decreased the elongation from 12.2 to 10.3% (16% decrease). Increase in strength may come from the refinement of structure and increase in fraction of hard Fe-IMCs in A356-Fe sample compared to A356 sample. Reduction in ductility is due to increased fraction of hard needle shaped Fe-IMCs which act as stress concentration points and may also crack during loading. In FSPed samples, however, considerable improvement in the tensile properties was observed compared to the cast samples. In Fe-free samples, FSP increases both strength and percent elongation from 162.1 MPa and 12.2% for A356 sample to 193.7 MPa (19% increase) and 28% (130% increase) for A356-FSP sample, respectively. In Fe-bearing samples, FSP increases both strength and percent elongation from 171.3 MPa and 10.3% for A356-Fe sample to 211.3 MPa (23% increase) and 25.4% (147% increase) A356-Fe-FSP sample, respectively. Coarse and elongated phases, such as-cast Si and Fe-IMC needles, tend to crack or interfacial separation early at tensile loading which result in reduction of both strength and ductility. Fracture can also start at defects such as casting pores. Hence, fragmented second phases in FSPed samples are less prone to fracture and interfacial separation and consequently show less detrimental effects on the tensile properties of the sample. In table (5), beside uniform elongation, values for total elongation were also reported. It can be seen that the cast samples, show up to 0.2% nonuniform elongation, which is negligible. In FSPed samples, however, 5 and 1.3% nonuniform elongation were observed for A356-FSP and A356-Fe-FSP which means that the FSPed samples shows considerable elongation after necking.

The fractured surfaces of the tensile test specimens, as shown in Figure 9, were studied to understand the fracture mechanism. According to Figure 9a1-a4, fractured surface of A356 sample shows features of mostly brittle fracture in which large facets (or cleavages) can be seen on the fractured surface. Large holes are also present which is indicated by the white arrows in image (a1). Dendrites can be seen inside the voids, Figure 9a3, which denotes the voids formed during solidification. Additionally, cracked Si needles can be readily seen in the fractured surface (black arrows). The fractured surface of A356-FSP sample, however, shows features of ductile fracture in which many dimples can be seen on the fractured surface. No casting voids and few cracked Si particles was observed on the fractured surface. Similar to sample A356, sample A356-Fe shows features of brittle fracture on its fractured surface, as presented in Figure 9c. Main difference to sample A356 is that instead of large casting voids, small holes are present on its fractured surface (white arrows in Figure 3c1. Many cracked needles can also be seen on the fractured surface (white arrows). Some of these cracked particles are Si needles and some of them are Fe-IMCs as proved by EDS point analysis results reported in Table 6. Fractured surface of A356-Fe-FSP is also shown the ductile fracture features, the same as A356-FSP sample.

Conclusion

In this study, effect of FSP on the microstructure, hardness, and tensile properties of standard A356 and A356-Fe (containing 1.2 wt.% Fe) alloys was investigated. The results proved the beneficial effects of FSP on the microstructure and mechanical properties of both alloys. The main results can be summarized as below.

 Addition of iron to A356 alloy significantly refined the as-cast structure and increased the fraction of Fe-IMCs and hence, slightly increased the strength, however, the ductility was significantly reduced.

- FSP completely changed the cast structure. The dendritic structure of cast alloys was vanished, and Si and Fe-IMC needles were fragmented to small particles.
- FSP considerably improved both strength and ductility of A356 and A356-Fe cast alloys.
- These results prove the beneficial effect of FSP on the structure and mechanical properties of ironbearing cast aluminum alloys. This is important in the view point of aluminum recycling industry as the Fe is the main impurity in these alloys.

Acknowledgements

The authors would gratefully acknowledge Dr. S.A. Hosseini for his delightful discussion on the XRD results.

Funding

This research did not receive any specific grant from funding agencies in the public, commercial, or not-for-profit sectors.

Conflict of interest The authors declare that they have no known competing financial interests or personal relationships that could have appeared to influence the work reported in this paper.

REFERENCES

- 1. P.R. Guru, F. Khan, S.K. Panigrahi, G.D.J. Ram, Enhancing strength, ductility and machinability of a Al-Si cast alloy by friction stir processing. J. Manuf. Process. **18**, 67–74 (2015). https://doi.org/10.1016/j.jmapro.2015.01.005
- M. Amne Elahi, S.G. Shabestari, Effect of various melt and heat treatment conditions on impact toughness of A356 aluminum alloy. Trans. Nonferrous Met. Soc. Chin. (English Ed) 26, 956–965 (2016). https:// doi.org/10.1016/S1003-6326(16)64191-2
- 3. H.R. Kotadia, M. Qian, A. Das, Microstructural modification of recycled aluminium alloys by high-intensity ultrasonication: observations from custom Al–2Si–2Mg–1.2Fe–(0.5,1.0)Mn alloys. J. Alloys Compd. **823**, 153833 (2020). https://doi.org/10.1016/j.iallcom.2020.153833
- J.A. Taylor, Iron-containing intermetallic phases in Al-Si based casting alloys. Proced. Mater. Sci. 1, 19–33 (2012). https://doi.org/10.1016/j.mspro.2012. 06.004
- X. Song, M. Gao, B. Yang, R. Guan, Modification and refinement of Fe-containing phases, mechanical properties and strengthening mechanisms in Al–Fe alloys via Cr alloying and continuous rheo-extrusion. Mater. Sci. Eng.: A 850, 143557 (2022). https://doi.org/10. 1016/j.msea.2022.143557
- 6. Z. Ma, A.M. Samuel, H.W. Doty, S. Valtierra, F.H. Samuel, Effect of Fe content on the fracture behaviour

- of Al-Si-Cu cast alloys. Mater. Des. **57**, 366–373 (2014). https://doi.org/10.1016/j.matdes.2014.01.037
- M. Kishor, K. Chopra, K.P.R. Ayyagari, Tackling Ferich intermetallics in Al-Si Alloy: a critical review. Trans. Indian Inst. Met. (2023). https://doi.org/10.1007/s12666-023-03205-8
- S.G. Shabestari, F. Shahri, Influence of modification, solidification conditions and heat treatment on the microstructure and mechanical properties of A356 aluminum alloy. J. Mater. Sci. 39, 2023–2032 (2004). https://doi.org/10.1023/B:JMSC.0000017764.20609. 0d
- F. Mao, G. Yan, Z. Xuan, Z. Cao, T. Wang, Effect of Eu addition on the microstructures and mechanical properties of A356 aluminum alloys. J. Alloys Compd. 650, 896–906 (2015). https://doi.org/10.1016/j.jall com.2015.06.266
- S. Derin, U. Aybarç, Y. Birol, Effect of strontium addition on microstructure and mechanical properties of AlSi7Mg0.3 alloy. Int. J. Metalcasting 11(4), 688–695 (2017). https://doi.org/10.1007/s40962-016-0117-4
- U.A. Curle, H. Möller, J.D. Wilkins, Shape rheocasting of unmodified Al-Si binary eutectic. Mater. Lett. 65, 1469–1472 (2011). https://doi.org/10.1016/j.mat let.2011.02.040
- S. Yadav, S.P. Tewari, J.K. Singh, S.C. Ram, Effects of mechanical vibration on the physical, metallurgical and mechanical properties of cast A308 (LM21) aluminum alloy. Int. J. Miner. Metall. Mater. 29, 1206–1215 (2022). https://doi.org/10.1007/s12613-020-2209-7
- S. Yadav, S. Kumar, S.P. Tewari, S.C. Ram, R. Prasad, M. Deo, J.K. Singh, Influence of high amplitude mould vibration on the morphology of silicon in the Al-Si alloy (A308). SILICON 15, 229–241 (2023). https://doi.org/10.1007/s12633-022-01997-w
- 14. E. Fracchia, F.S. Gobber, M. Rosso, Effect of alloying elements on the Sr modification of Al-Si cast alloys. Metals (Basel). **11**, 1–19 (2021). https://doi.org/10.3390/met11020342
- M.H. Khan, A. Das, Z. Li, H.R. Kotadia, Effects of Fe, Mn, chemical grain refinement and cooling rate on the evolution of Fe intermetallics in a model 6082 Alalloy. Intermetallics 132, 1–10 (2021). https://doi.org/ 10.1016/j.intermet.2021.107132
- Y.-C. Tzeng, W. Chih-Ting, H.-Y. Bor, J.-L. Horng, M.-L. Tsai, S.-L. Lee, Effects of scandium addition on iron-bearing phases and tensile properties of Al–7Si– 0.6Mg alloys. Mater. Sci. Eng.: A 593, 103–110 (2014). https://doi.org/10.1016/j.msea.2013.11.039
- M. Wang, W. Xu, Q. Han, The influence of sr addition on the microstructure of a380 alloy. Int. J. Met. 11, 321–327 (2017). https://doi.org/10.1007/s40962-016-0071-1

- K.K. Jlood, M.K. Abbass, M.M. Hanoon, Effect of friction stir processing parameters on microstructure and mechanical properties of aluminum alloy AA6061-T6: experimental and statistical study. Salud, Ciencia y Tecnología - Serie de Conferencias 3, 862 (2024). https://doi.org/10.56294/sctconf2024862
- M.K. Abbass, N.A.B. Sharhan, Characteristics of Al6061-SiC-Al2O3 surface hybrid composites fabricated by friction stir processing. J. Mater. Eng. 1(4), 147–158 (2023). https://doi.org/10.61552/JME.2023. 04.002
- R. Prasad, H. Kumar, N.K. Sinha, S.P. Tewari, J.K. Singh, S. Yadav, M. Deo, Characterization of A356/ (fly ash+ red mud) surface hybrid composite fabricated by friction stir processing. Mater. Today Proc. 46, 1476–1480 (2021). https://doi.org/10.1016/j.matpr.2020.10.889
- M.K. Abbass, N.A. Baheer, Effect of SiC Particles on Microstructure and Wear Behavior of AA6061-T6 Aluminum Alloy Surface Composite Fabricated by Friction Stir Processing, IOP Conf. Ser. Mater. Sci. Eng. 671 (2020). https://doi.org/10.1088/1757-899X/ 671/1/012159.
- 22. Z.Y. Ma, S.R. Sharma, R.S. Mishra, Effect of friction stir processing on the microstructure of cast A356 aluminum. Mater. Sci. Eng.: A **433**(1–2), 269–278 (2006). https://doi.org/10.1016/j.msea.2006.06.099
- 23. Z.Y. Ma, S.R. Sharma, R.S. Mishra, Microstructural modification of As-cast Al-Si-Mg alloy by friction stir processing. Metal. Mater. Trans. A **37**(11), 3323–3336 (2006). https://doi.org/10.1007/BF02586167
- S. Meenia, F. Khan, S. Babu, R.J. Immanuel, S.K. Panigrahi, G.D. Janaki Ram, Particle refinement and fine-grain formation leading to enhanced mechanical behaviour in a hypo-eutectic Al-Si alloy subjected to multi-pass friction stir processing. Mater. Charact. 113, 134–143 (2016). https://doi.org/10.1016/j.matchar.2016.01.011
- M. Akbari, P. Asadi, Effects of different cooling conditions on friction stir processing of A356 alloy: numerical modeling and experiment. Proc. Inst. Mech Eng. Part C J. Mech. Eng. Sci. 236, 4133–4146 (2022). https://doi.org/10.1177/09544062211045655
- N. Sun, D. Apelian, Friction stir processing of aluminum alloy A206: part I—microstructure evolution. Int. J. Met. 13, 234–243 (2019). https://doi.org/ 10.1007/s40962-018-0263-y
- 27. N. Sun, W.J. Jones, D. Apelian, Friction stir processing of aluminum alloy A206: part ii—tensile and fatigue properties. Int. J. Met. **13**, 244–254 (2019). https://doi.org/10.1007/s40962-018-0268-6
- 28. S. Caizhi, L. Hui, W. Feng, H. Xudong, H. Wei, S. Volodymyr, Study on the microstructure and mechanical properties of ZrB2/AA6111 particle-reinforced aluminum matrix composites by friction stir processing and heat treatment. Int. J. Met. 18,

- 457–469 (2024). https://doi.org/10.1007/s40962-023-01029-2
- A. Heidarzadeh, M. Khorshidi, R. Mohammadzadeh, R. Khajeh, M. Mofarrehi, M. Javidani, X.G. Chen, Multipass friction stir processing of laser-powder bed fusion AlSi10Mg: microstructure and mechanical properties. Materials (Basel). (2023). https://doi.org/ 10.3390/ma16041559
- 30. X. Ai, Y. Yue, Microstructure and Mechanical properties of friction stir processed A356 cast Al under air cooling and water cooling. High Temp. Mater. Process. **39**, 41–47 (2018). https://doi.org/10.1515/htmp-2017-0036
- 31. V. Abouei, S.G. Shabestari, H. Saghafian, Dry sliding wear behaviour of hypereutectic Al-Si piston alloys containing iron-rich intermetallics. Mater Charact **61**, 1089–1096 (2010). https://doi.org/10.1016/j.matchar. 2010.07.001
- C. Bidmeshki, V. Abouei, H. Saghafian, S.G. Shabestari, M.T. Noghani, Effect of Mn addition on Fe-rich intermetallics morphology and dry sliding wear investigation of hypereutectic Al-175%Si alloys. J. Mater. Res. Technol. 5, 250–258 (2016). https://doi.org/10.1016/j.jmrt.2015.11.008
- V. Abouei, H. Saghafian, S.G. Shabestari, M. Zarghami, Effect of Fe-rich intermetallics on the wear behavior of eutectic Al-Si piston alloy (LM13). Mater. Des. 31, 3518–3524 (2010). https://doi.org/10.1016/j.matdes.2010.02.015
- M. Shamanian, H. Mostaan, M. Safari, J.A. Szpunar, EBSD study on grain boundary and microtexture evolutions during friction stir processing of A413 cast aluminum alloy. J. Mater. Eng. Perform. 25, 2824–2835 (2016). https://doi.org/10.1007/s11665-016-2141-1
- B. Suárez-Peña, J. Asensio-Lozano, Influence of Sr modification and Ti grain refinement on the morphology of Fe-rich precipitates in eutectic Al-Si die cast alloys. Scr. Mater. 54, 1543–1548 (2006). https:// doi.org/10.1016/j.scriptamat.2006.01.029
- A. Školáková, P. Novák, D. Vojtěch, T.F. Kubatík, Microstructure and mechanical properties of Al-Si-Fe-

- X alloys. Mater. Des. **107**, 491–502 (2016). https://doi.org/10.1016/j.matdes.2016.06.069
- 37. G.R. Cui, D.R. Ni, Z.Y. Ma, S.X. Li, Effects of friction stir processing parameters and in situ passes on microstructure and tensile properties of Al-Si-Mg casting, metall. Mater. Trans. A Phys. Metall. Mater. Sci. 45, 5318–5331 (2014). https://doi.org/10.1007/s11661-014-2494-8
- 38. R. Mishra, Z. Ma, Friction stir welding and processing. Mater. Sci. Eng. R **50**, 1–78 (2005)
- 39. A. Arora, Z. Zhang, A. De, T. DebRoy, Strains and strain rates during friction stir welding. Scr. Mater. **61**, 863–866 (2009). https://doi.org/10.1016/j.scriptamat. 2009.07.015
- J. Han, J. Chen, L. Peng, F. Zheng, W. Rong, Y. Wu, W. Ding, In fluence of processing parameters on thermal field in Mg–Nd–Zn–Zr alloy during friction stir processing. Mater. Des. 94, 186–194 (2016). https://doi.org/10.1016/j.matdes.2016.01.044
- 41. C.H. Cáceres, C.J. Davidson, J.R. Griffiths, The deformation and fracture behaviour of an AlSiMg casting alloy. Mater. Sci. Eng. A **197**, 171–179 (1995). https://doi.org/10.1016/0921-5093(94)09775-5
- M. Tiryakioğlu, J. Campbell, J.T. Staley, The influence of structural integrity on the tensile deformation of cast Al–7wt.%Si–0.6wt.%Mg alloys. Scr. Mater.
 49, 873–878 (2003). https://doi.org/10.1016/S1359-6462(03)00439-1

Publisher's Note Springer Nature remains neutral with regard to jurisdictional claims in published maps and institutional affiliations.

Springer Nature or its licensor (e.g. a society or other partner) holds exclusive rights to this article under a publishing agreement with the author(s) or other rightsholder(s); author self-archiving of the accepted manuscript version of this article is solely governed by the terms of such publishing agreement and applicable law.